SPECIAL ISSUE PAPER

Simultaneous estimation of elasticity for multiple deformable bodies

Shan Yang* and Ming Lin

Department of Computer Science, University of North Carolina at Chapel Hill, Brooks Computer Science Building 201 S. Columbia St., Chapel Hill, NC, USA

ABSTRACT

Material property has great importance in deformable body simulation and medical robotics. The elasticity parameters, such as Young's modulus of the deformable bodies, are important to make realistic animations.

Further, in medical applications, the (recovered) elasticity parameters can assist surgeons to perform better pre-op surgical planning and enable medical robots to carry out personalized surgical procedures. Previous elasticity parameters estimation methods are limited to recover one elasticity parameter of one deformable body at a time. In this paper, we propose a novel elasticity parameter estimation algorithm that can recover the elasticity parameters of multiple deformable bodies or multiple regions of one deformable body simultaneously from (at least two sets of) images. We validate our algorithm with both synthetic test cases and real patient computed tomography images. Copyright © 2015 John Wiley & Sons, Ltd.

KEYWORDS

elasticity parameter reconstruction; human tissue simulation; tissue material property

All supporting information may be found in the online version of this article.

*Correspondence

Shan Yang, University of North Carolina at Chapel Hill.
E-mail: alexyang@cs.unc.edu

1. INTRODUCTION

Material properties are important in depicting the characteristics of virtual objects for realistic computer animations of soft bodies.

In addition, virtual surgical simulation has also been increasingly used for rapid prototyping of clinical devices, pre-operation planning of medical procedures, virtual training exercises for surgeons and medical personnel, and so on. And, tissue elasticity properties are important parameters for developing accurate and predictive surgical simulation. Furthermore, to compute desired and accurate force feedback for haptic display requires knowledge about the deformation of soft tissues and organs, which are characterized by patient-specific elastic parameters for different tissues and organs.

Elastography[1] was first proposed to determine the elasticity properties by measuring the deformation of the tissue because of the application of the known external forces. The known external forces are the boundary condition needed to recover the exact elasticity parameter. Originally, the deformations were measured using ultrasound imagery[2], but such techniques produced coarse,

two-dimensional representations of the moving tissue. More sophisticated imaging techniques, such as magnetic resonance imaging (MRI)[3,4] and computed tomography (CT), produce three-dimensional images of the deforming tissues, allowing a more accurate measurement of displacement.

Toward realizing the concept of three-dimensional physiological humans, we propose perhaps one of the first elasticity parameter estimation algorithm for *multiple, heterogeneous* deformable bodies simultaneously using medical images[†]. Our approach is based on a multi-dimensional optimization method that iteratively performs deformable body simulation using a finite element (FE) method on reconstructed organ models with the continuously refined, estimated elasticity parameters. The geometric models of organs are reconstructed based on low-resolution CT images.

Our objective function measures the sum of the distance between the nodes of the organ surface. In contrast to

---

[†]In this paper, we use CT images. But, the algorithm is also applicable to MRI images.

elastography methods [5–7], the only information we need is the displacement of the nodes of the organ surface. We do not need every pixel-wise displacement vector, thus, no extra procedures need to be performed on the patient. Two sets of (medical) images are sufficient to recover the elasticity parameters using our method. Therefore, our method can be widely applicable to different imaging technology. It can be used for animatino of soft bodies (see supplementary video) and possibly for cancer staging using only low-resolution CT images.

2. RELATED WORK

In computer graphics, extensive research has been done for deformable body simulation [8–11]. Researchers have also been studying methods for designing simulation with material properties [12–15] and for realistic bio-structure simulation [16].

In medical applications, there are mainly two kinds of soft tissue elasticity properties estimation methods [17]: invasive and noninvasive techniques. The invasive methods rely on a device to measure the displacement and force response [18–20]. These methods take organ samples either out of the human or animal bodies and perform the experiment *in vitro* (out side the body) or do the procedure *in situ* (inside the body). The collected data are then used to solve the inverse problem, which is to recover the elasticity properties, by constructing a polynomial interpolation [21] or by using an FE model [17,22,23].

The noninvasive methods were mostly based on image analysis techniques to measure the displacement. In the 1980s, several methods were proposed to measure the motion of the soft tissue, such as the one proposed by Wilson and Robinson [24] using radio frequency M-mode signals and the one proposed by Birnholz and Farrell [25] using ultrasound B-scans. Researchers have also used medical image analysis on 2-D ultrasound and/or MRI images to estimate the elastic parameters of soft tissue [26–28].

In the area of elastography, researchers [5–7] proposed algorithms based on the distance between two medical images. By solving the least square problem, the elasticity parameters are recovered. Van Houten *et al.* [4] used elastography methods to estimate the Young's modulus distribution of a 2D area, then later extended to solve three-dimensional elastic parameter distribution using MRI [29]. These methods need high-resolution displacement fields to recover the elasticity parameter [27], where the displacement field is typically obtained through an external device using a vibration actuation mechanism. For organs that are located deep-seated inside a human body, the vibrator may need to be placed inside the organ[30], making the procedure much more complex and possibly uncomfortable for the patient.

Other than distance field based methods, there are also other measurement algorithms. The modality-independent elastography method [31] measures the elasticity parameters by maximizing the image similarity based on a number of landmarks. However, this technique does not apply to all the soft tissues, as landmarks cannot always be found in some of the organs such as prostate. Statistical and machine learning algorithms have also been used to classify soft tissues and estimate the parameters using multi-spectral MR images [32].

Although the existing elastography methods can provide an estimation of the elasticity parameter distribution, they require high-resolution magnetic resonance medical images and a device to measure the external force exerted on the soft tissues, which is not always possible or practical. Lee *et al.* proposed the first model to estimate the Young's modulus based on low-resolution CT images, and no external force is needed to set the boundary condition [33]. By optimizing the distance between the deformed and the reference surface meshes, the elastic parameter is estimated. However, this method can only recover the elasticity parameter of one organ. In contrast, our work can recover the elasticity parameters of *multiple, heterogeneous* soft bodies *simultaneously*, using a multi-dimensional optimization method.

3. METHOD

We propose a novel method to automatically estimate elasticity parameters of multiple organs using only images, such as those from CT imaging. Our approach is based on multi-dimensional optimization and simulation of multiple deformable bodies using FE methods. For each optimization iteration, an FE method is used to assess the deformation of the organs. The objective function is based on distance between the initial, reference mesh, and the deformed surface mesh. This objective function is evaluated and its gradient is used in the multi-dimensional optimization algorithm to search for the optimized elasticity parameters that minimize the value of the objective function. The flow chart of the optimization process is shown in Figure 1.

A three-dimensional reconstructed model of the organs and the signed distance map of the deformed organs are the input of our algorithm. The three-dimensional model is reconstructed from the segmented CT images using ITK-SNAP [34]. After each optimization iteration, the elasticity parameters are updated and used by the FE model. The simulation-based parameter estimation algorithm is terminated when the optimization converges, which usually takes only a few iterations.

3.1. Forward Simulation

The forward simulation in our method computes the displacement vector **u** using the elasticity parameters recovered in the inverse problem.

The displacement vector **u** is then used in the inverse problem to evaluate the objective distance function Equation (4). Our simulation framework uses a linear static
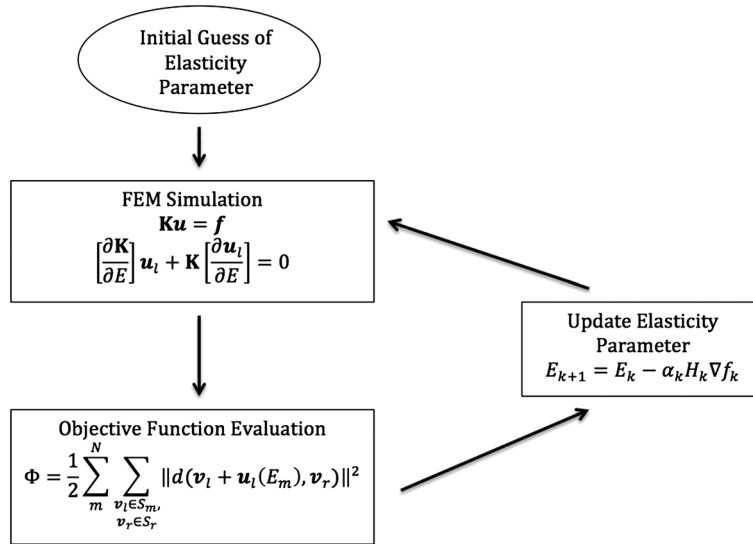
Figure 1. The flow chart of the optimization iteration. The initial guess of the elasticity parameter is provided based on standard tissue values, prior to the start of the optimization. For each optimization iteration, the tissue deformation is recomputed using a finite element (FE) method simulation. The value of the distance objective function is also re-evaluated. At the end of each iteration, the elasticity parameter is updated and used by the FE model to continue the simulated-based optimization process.

FE method [35] (Equation (1)). The weak formulation for elasticity problem is given,

$$\int_\Omega \nabla \mathbf{u}^T \rho \ddot{\mathbf{u}} d\Omega + \int_\Omega \nabla \epsilon^T \boldsymbol{\sigma} d\Omega - \int_\Omega \nabla \mathbf{u}^T \mathbf{b} d\Omega - \int_\Gamma \nabla \mathbf{u}^T \mathbf{t} d\Gamma = 0 \qquad (1)$$

where $\mathbf{u}$ is the displacement vector and $\mathbf{t}$ is the boundary condition(traction act on the boundary Γ). For quasi-static deformation process, the $\ddot{\mathbf{u}} = 0$. We can rewrite Equation (1) as

$$\left[\int_\Omega \nabla \epsilon^T \sigma d\Omega - \int_\Omega \nabla \mathbf{u}^T \mathbf{b} d\Omega \right] - \left[\int_\Gamma \nabla \mathbf{u}^T \mathbf{t} d\Gamma \right] = 0 \qquad (2)$$

with the first part of the equation as the internal force and the second part of the equation as the external force.

We use linear elastic material model. For isotropic linear elasticity, the stress–strain relation is defined as,

$$\sigma = \mathbf{D}\varepsilon \qquad (3)$$

where σ is the stress tensor, ε is the strain tensor, and matrix $\mathbf{D}$ is defined by the material elasticity parameters. We use Young's modulus E and Poisson's ratio ν for describing material properties.
Previous elastography methods use external forces as the boundary condition. Our method, in contrast, does not need external forces. The initial boundary condition in our algorithm is the known displacement vector of the surface mesh. This boundary condition is applied only to the nodes of the surface mesh. When the three-dimensional model deformed, the force generated by the deformation will drive the simulation.

3.2. The Inverse Problem

The inverse problem is the process of elasticity parameter estimation. Our method is based on the multi-dimensional optimization method. By solving the least square problem iteratively, we recover the elasticity parameter. We then use the distance between the initial, reference surface mesh, and the deformed surface mesh to iteratively update the objective function.

3.2.1. Distance Based Objective Function.

As our simulation framework is based on the low-resolution CT images, only the displacement of the boundary of the soft tissue is known. Our objective function Equation (4) is constructed using the sum of the distance between the nodes of initial, reference surface, and that of the deformed surface. By minimizing the value of the objective function, we find the optimal elasticity parameters $\boldsymbol{\mu}$.

$$\Phi(\mu_m) = \frac{1}{2} \sum_{m=1}^{N} \sum_{\mathbf{u}_l \in S_m, \mathbf{u}_r \in S_r} \|d(\mathbf{u}_l + \Delta\mathbf{u}_l, \mathbf{u}_r)\|^2 \qquad (4)$$

where m is the mth organ and N is the number of organs that is in the simulation scene.
$d(\mathbf{u}_l + \Delta\mathbf{u}_l, \mathbf{u}_r)$ is the bidirectional Hausdorff distance between deformed surface mesh S_m and the initial, reference mesh S_r. $\mu_m = E_m$, in which E_m is the Young's modulus of the mth organ. Our method can be extended to optimize more than one parameter. We could also include the Poisson's ratio into μ_m.
The μ that minimizes the objective function is the optimized set of elasticity parameters.

3.2.2. Multi-Dimensional Numerical Optimization Method.

We propose to use a multi-dimensional optimization method to recover the elasticity parameters. Our three-dimensional model can have a large number of nodes, so a significant amount of memory would be needed to store the exact Hessian matrix for the Newton's optimization method. Therefore, to solve the least square problem, we choose the Limited Memory Quasi-Newton's method.

Using this method, the approximation of the Hessian matrix is maintained instead of the exact Hessian matrix. For each step of this Broyden–Fletcher–Goldfarb–Shanno method [36],

$$\mu_{k+1} = \mu_k - \alpha_k H_k \nabla \Phi_k \qquad (5)$$

where H_k is the approximated Hessian matrix, $\mathbf{x}_k$ is the variable to be optimized, Φ_k is the objective function value, k denotes the kth optimization iteration, and $\nabla \Phi$ is the gradient of the objective function. To compute the gradient, the partial derivative of Φ is with respect to the elasticity parameter, the Young's modulus of the mth organ.

4. EXPERIMENT

We have implemented our algorithm and performed three sets of experiments to evaluate its accuracy under different conditions using both two synthetic sets of models with known parameters to validate the approach and a reconstructed set of organs from CT images to illustrate its robustness.

4.1. Recovering Known Values

The first experiment is designed to test the accuracy of the algorithm, if the three organs sharing boundary. As the number of the organs increases, the problem becomes even more complicated.

4.1.1. Model Construction.

We used 3-concentric spheres to build the test model in experiment I. In order to measure the elastic parameter of sphere 1, for the area between sphere 1 and sphere 2 and the area between sphere 2 and sphere 3, tetrahedralization is carried out within sphere 1, the area between sphere 1 and sphere 2 and the area between sphere 2 and sphere 3. The sliced view of the three-dimensional model is shown in Figure 2. The following table is generated when the three areas are all deformed by slightly less than 10%.

4.1.2. Result.

The result of this experiment is shown in Table I. In this experiment we increase the number of "organs" to test the accuracy of our algorithm. The result of this experiment is affected by both the fact that the spheres are sharing
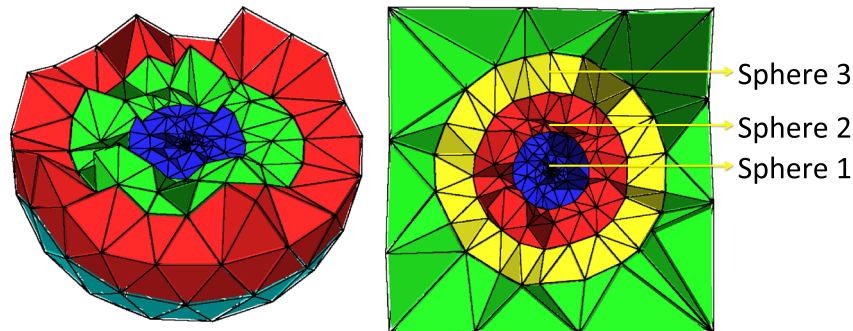
Figure 2. A sliced view of the tetrahedral mesh of experiment I. The image on the left shows only the tetrahedral mesh of the spheres, while the image on the right shows the complete tetrahedral mesh.

Table I.

True elasticity (kPa)	Initial guess (kPa)	Sphere 1		Sphere 2		Sphere 3	
		Recovered value	Relative error (%)	Recovered value	Relative error (%)	Recovered value	Relative error (%)
50	25	49.23	1.54	49.54	0.92	49.55	0.9
70	35	66.14	5.51	67.41	3.7	67.15	4.07
90	45	89.18	0.91	89.52	0.53	89.68	0.36
110	55	107.93	1.88	108.76	1.13	109.17	0.75
130	65	112.89	13.16	118.95	8.5	124.89	3.93
150	750	132.87	11.44	138.78	7.48	145.32	3.12

The true elasticity value, the Young's modulus is the one we provided to deform the model. Sphere 1, the area between sphere 1 and sphere 2, and the area between sphere 2 and sphere 3 are the three "organs" that we experimented on. The recovered elasticity parameters and the relative errors are shown in this table.
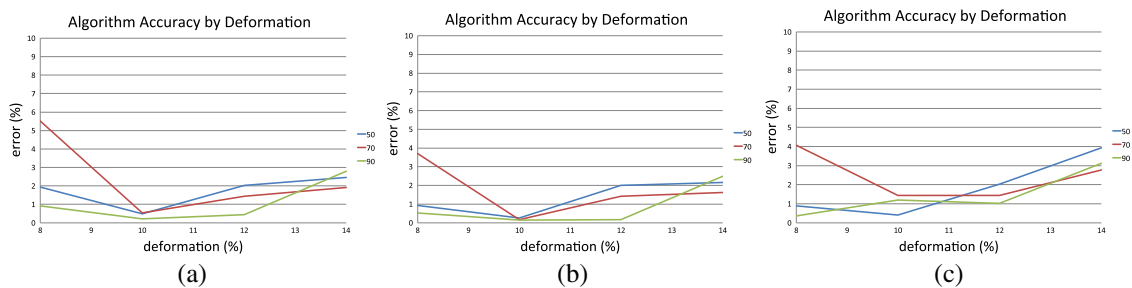
Figure 3. In this experiment, we show the relative errors (in %) of our algorithm versus the amount of deformation of sphere 1 (left), sphere 2 (middle), and sphere 3 (right). The three lines represent the experiment result with different ground truth elasticity values.

boundaries and the number of the spheres. Under these complicated conditions, the error rate of our algorithm is generally less than 5% (no more than 15% for the highest stiffness values) when the deformation is less than 10% within each of the three regions, respectively (Figure 3).

4.2. Multiple Reconstructed Organs

The second experiment is designed to test the robustness of our algorithm with more scenes that consist of multiple, separate organs in contact with each other. The simulation scene includes multiple organs within a male's pelvis area. The surface meshes of the prostate, bladder, and rectum were reconstructed from the patient's CT images. These reference surface meshes were used to construct the tetrahedral mesh of the simulated scene. A slice view of the tetrahedral mesh is shown in Figure 4. In the tetrahedral mesh, the rectum was modeled hollow inside, while the prostate and the bladder were modeled as a continuum represented by tetrahedral elements. The prostate and the bladder are two organs that we use to recover the elasticity parameters.

The signed distance field within each organ was computed using the initial, reference surface mesh and the deformed surface mesh. The deformed surface mesh was generated based on the displacement of the nodes on the surface mesh. We used the initial displacement to set the initial forces as the boundary condition. Then the boundary condition was used to generate a displacement field,

which was computed by applying the boundary condition to the three-dimensional model during each iteration of the optimization. The model was deformed using the current set of elasticity parameters. For the synthetic test case, we generate the deformed surface by using the set of "ground truth" parameters. We then run our algorithm on the resulting deformed surface to estimate the elasticity parameters and compare these recovered values with the ground-truth values, as shown in Table II.

In the experiment, we fixed the Poisson's ratio of the material, which only optimized the Young's modulus of the organs. The choice of Poisson's ratio was taken from the literature [37–39].

4.2.1. Model Construction.

We use patient specific medical images to reconstruct the organ models. The CT images were segmented using ITK-SNAP [34]. After segmentation, we reconstruct the surface mesh of the prostate, bladder, and rectum also using ITK-SNAP [34]. The surface meshes are shown in Figure 5. Then, we used TetGen [40] to generate the tetrahedral mesh based on the surface mesh of the organs and a bounding box, with the rectum being hollow inside shown in Figure 6. We used the deformation of the rectum to set the boundary condition. The deformed prostate and the bladder surface mesh are used to compute the updated, signed distance map.

Table II.

		Prostate		Bladder	
True elasticity (kPa)	Initial guess (kPa)	Recovered value	Relative error (%)	Recovered value	Relative error (%)
50	25	53.28	6.56	49.67	0.66
100	50	107.50	7.5	97.78	2.22
150	75	157.53	5.02	146.49	2.34
200	100	209.08	4.54	198.07	0.97
250	125	263.30	5.32	248.60	0.56
300	150	315.14	5.04	296.86	1.04

The true elasticity value, the Young's modulus is the one we provided to deform the model. We recover the elasticity of both the prostate and the bladder. Their recovered elasticity and the relative errors are also shown in this table.

4.2.2. Result.

We first did a search of the initial relative Young's Modulus. The initial value affects the optimization result, and several initial values are used to ensure convergence and determine the global minima. The experimental result is shown in Table II. In our experiment, we initially assigned the same Young's modulus to both organs, the prostate, and the bladder. The three-dimensional models are deformed based on the boundary condition we provided and the Young's modulus we assigned to the two organs. The boundary condition was defined according to the two surface meshes, which were constructed using two CT images taken from the same patient in different times. From the table, we can observe that the relative errors of the bladder are generally smaller than those of the prostate. From [41], we know that the stiffness of the cancer tissue tend to be much more than 10% of the normal tissue, while the error of our algorithm is less than 10% in all early cases. Thus, given the relative errors of our algorithm, it can still detect cancer. This result also

shows the limitation of the linear elastic material model. The accuracy is affected by the amount of deformation of the organs.

4.3. Application to Cancer Staging

We use multiple sets of CT images from each of eight patients (totaling 180 sets of images) in our real cancer correlation experimental study. The simulation scene, which includes multiple organs within a male's pelvis area, is the same as the second experiment.

The experiment is designed to determine the correlation between the prostate cancer T stage and the elasticity of prostate and the surrounding organs. The T-stage is defined in the tumor, nodes, metastasis system[42], which is a common cancer staging system.

The result of our experiment is shown in Figures 7 and 8. Using the box plot, we can observe that the mean of both the prostate's and the bladder's Young's increases with the cancer staging (the resulting Young's modulus
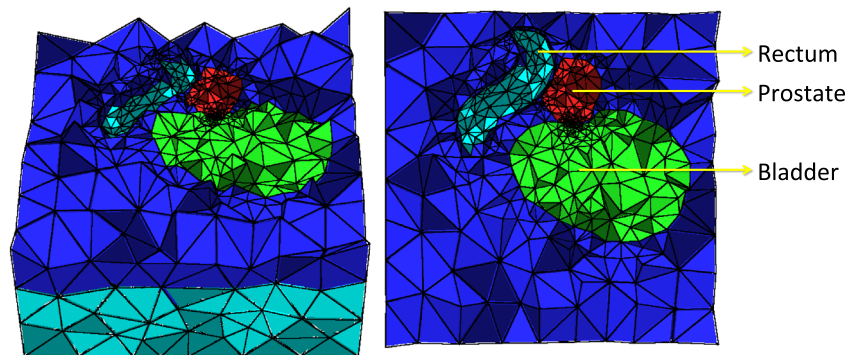
Figure 4. A sliced view of the tetrahedral mesh.
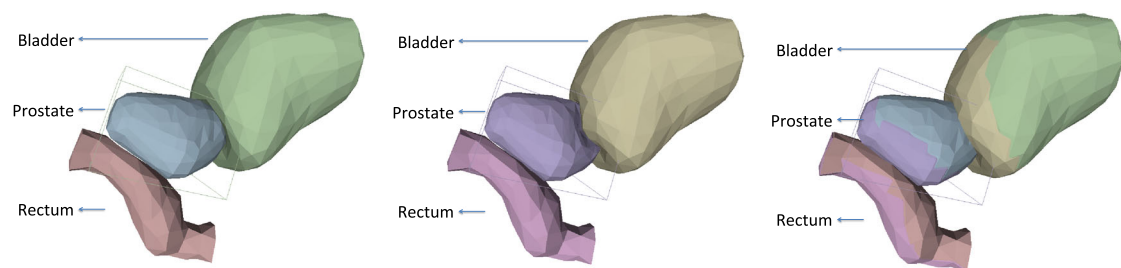
(a) The reference surface meshes of the rectum, the prostate and the bladder.

(b) The deformed surface meshes of the rectum, the prostate and the bladder.

(c) The combined view of the reference and the deformed surface meshes of multiple organs.

Figure 5. (a) Reference surface mesh, (b) deformed surface mesh using the elasticity parameter we provided, and (c) deformation from reference meshes to the deformed meshes.
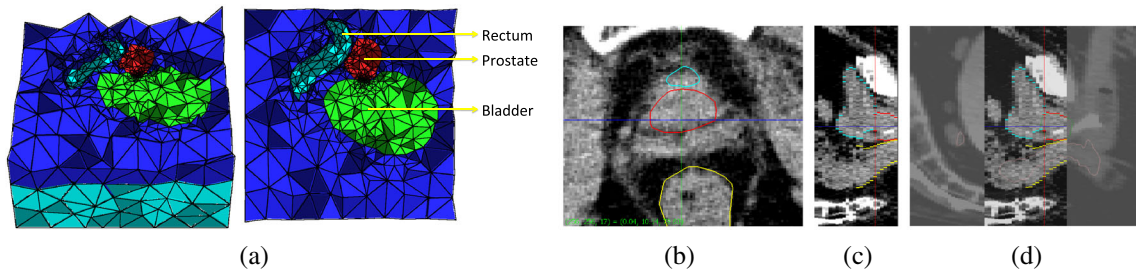
Figure 6. (a) The reconstructed three-dimensional tetrahedral mesh; (b), (c), and (d) present the segmentation result of the CT image of the pelvis area in which the red, green and yellow circles show the prostate, bladder, and rectum.

is the average value of the entire organ). We further analyze the statistical significance of this correlation between the T-stages and the elasticity of prostate and bladder. The resulting Pearson correlation coefficient for prostate's Young's modulus and T-stage is 0.658 and the p-value for two-tailed probability is 0.0000316, which indicate a

strong correlation between the Young's modulus of the prostate and the cancer T-stage. The resulting Pearson correlation coefficient for bladder Young's modulus and T-stage is 0.481 and the p-value for two tailed probability is 0.00460. This result indicates that the Young's modulus of the bladder increases with the stages of prostate cancer,
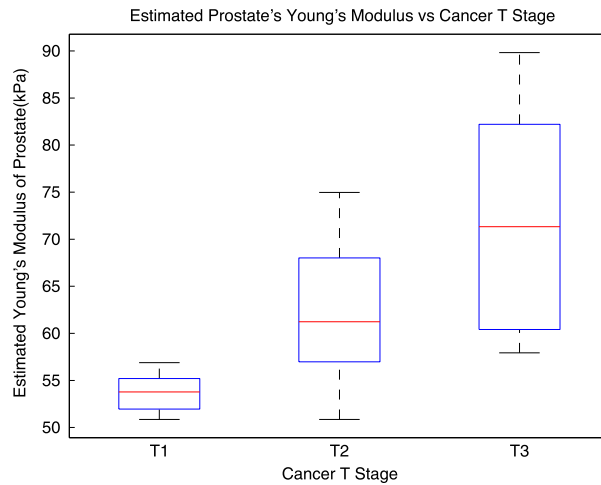
Figure 7. Box plot of the estimated Young's Modulus of the prostate of the eight patients.
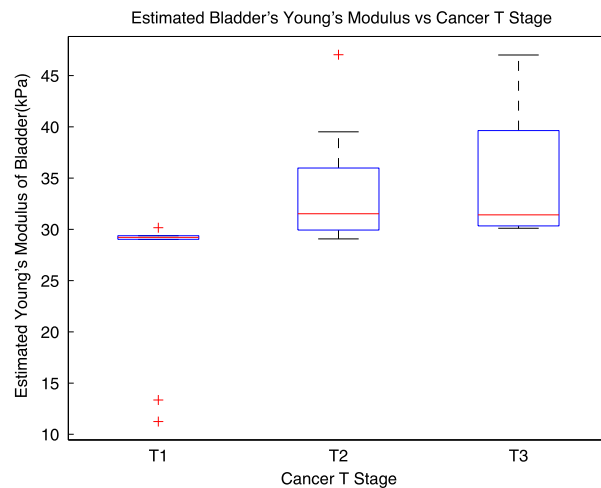
Figure 8. Box plot of the estimated Young's Modulus of the bladder of the eight patients.

but they are not strongly correlated. Our findings reconfirm the studies [43] that prostate cancer increases the probability of bladder cancer. As cancer continues to advance to higher stages, it spreads to neighboring tissues.

4.4. Discussion

We have used a range of deformation that is larger than the normal tissue deformation to stress test our algorithm and to analyze the relationship between the degree of accuracy versus the amount of deformation. This analysis helps us understand when nonlinear models should be used. Additional sensitive analysis with respect to segmentation, simulation resolution (i.e. the size of mesh), and use of nonlinear FEM model can also be performed to provide additional information to the users. We "jumpstart" the iterative optimization process with some range of default values and the algorithm usually converges quickly within less than 10 iterations in practice.

Our implementation currently addressed the possibility of multiple solutions by using multiple (3–5) initial values sampled over a wide range (50–300) of possible values (say 50, 150, 250) and use multiple sets of the image data from few different days to compute the average values, after eliminating possible "outliner value(s)". With this approach, our algorithm is able to find the elasticity parameters that are very close to the "ground truth" values in practice.

5. CONCLUSION AND FUTURE WORK

In this paper, we presented a novel multi-body elasticity parameter estimation method using low-resolution CT images. As our method do not require any external forces to be measured and only the deformation of the organ surface is needed, it can be applied to organs that are located deep-seated in the human body. There are limitations, however. The amount of deformation of the soft tissue can affect the accuracy of the algorithm. The larger the deformation, the higher the relative error is from the estimation. This is because of the fact that we have adopted a linear, static FE method and linear elastic material model. Linear models are generally considered accurate and sufficient when the deformation is small and within a certain range where linearity assumption is applicable. Our experimental results support this observation. The linear elastic material model is not suitable for the simulation of human organs when they undergo a large deformation. In the future, we plan to adopt a more complex, nonlinear elastic material model for soft tissue simulation, such as the Mooney Rivlin model. The accuracy may likely be higher when the amount of deformation is significant, although we expect the computation cost to increase as well.

The algorithm we proposed in this paper is based on a multi-dimensional optimization method, which can also be used to estimate multiple elasticity parameters of a single organ of multiple, heterogeneous tissue properties for different regions of a (human) body. Because of the importance of Young's modulus in noninvasive cancer detection, we choose to estimate this parameter for multiple organs simultaneously. However, Poisson's ratio has also been suggested as a significant indicator for breast cancer. Therefore, in the future, we plan to further study the accuracy of multi-dimensional optimization method and hope to use it to estimate multiple elasticity parameters of a single organ for more accurate cancer screening and grading.

ACKNOWLEDGEMENTS

REFERENCES

1. Ophir J, Céspedes I, Ponnekanti H, Yazdi Y, Li X. Elastography: a quantitative method for imaging the elasticity of biological tissues. *Ultrasonic Imaging* 1991; **13**(2): 111–134.

2. Krouskop TA, Dougherty DR, Vinson, FS, *et al*. A pulsed Doppler ultrasonic system for making noninvasive measurements of the mechanical properties of soft tissue. *Journal of Rehabilitation Research and Development* 1987; **24**(2): 1–8.

3. Chenevert TL, Skovoroda AR, Odonnel M, Emelianov SY. Elasticity reconstructive imaging by means of stimulated echo MRI. *Magnetic Resonance in Medicine* 1998; **39**(3): 482–490.

4. Van Houten EEW, Paulsen KD, Miga MI, Kennedy FE, Weaver JB. An overlapping subzone technique for MR-based elastic property reconstruction. *Magnetic Resonance in Medicine* 1999; **42**(4): 779–786.

5. Becker M, Teschner M. Robust and efficient estimation of elasticity parameters using the linear finite element method. *Proceedings of Simulation and Visualization* 2007: 15–28.

6. Eskandari H, Salcudean SE, Rohling R, Bell I. Real-time solution of the finite element inverse problem of viscoelasticity. *Inverse Problems* 2011; **27**(8): 085002.

7. Zhu Y, Hall TJ, Jiang J. A finite-element approach for Young's modulus reconstruction. *Medical Imaging, IEEE Transactions on* 2003; **22**(7): 890 –901.

8. Terzopoulos D, Platt J, Barr A, Fleischer K. Elastically deformable models 1987; **21**: 205–214.

9. Nealen A, Muller M, Keiser R, Boxerman E, Carlson M. Physically based deformable models in computer graphics. *Computer Graphics Forum* 2006; **25**: 809–836.

10. Müller M, Gross M. Interactive virtual materials. In *Proceedings of Graphics Interface 2004, GI '04*, School of Computer Science, University of Waterloo, Waterloo, Ontario, Canada, 2004, Canadian Human-Computer Communications Society; 239–246.

11. Meehan M, Teschner M, Girod S. Three-dimensional simulation and prediction of craniofacial surgery. *Orthodontics & Craniofacial Research* 2003; **6**(s1): 102–107.

12. Miguel E, Bradley D, Thomaszewski, B, *et al*. Data-driven estimation of cloth simulation models. *Computer Graphics Forum (Eurographics 2012)* 2012; **31**(2): 519–528.

13. Miguel E, Tamstorf R, Bradley, E, *et al*. Modeling and estimation of internal friction in cloth. *ACM Transactions on Graphics (Proc. SIGGRAPH Asia)* 2013; **32**(6).

14. Wang H, Ramamoorthi R, O'Brien J. Data-driven elastic models for cloth: modeling and measurement. *ACM Transactions on Graphics (SIGGRAPH)* 2011; **30**(4): 71:1–71:12.

15. Bickel B, Bächer M, Otaduy, MA, *et al*. Design and fabrication of materials with desired deformation behavior. In *ACM SIGGRAPH 2010 Papers*, Los Angeles, California, 2010; 1–10.

16. Maciel Anderson, Boulic Ronan, Thalmann Daniel. Deformable tissue parameterized by properties of real biological tissue. In *Surgery Simulation and Soft Tissue Modeling*. Springer: Springer Berlin Heidelberg, 2003; 74–87.

17. Samur E, Sedef M, Basdogan C, Avtan L, Duzgun O. A robotic indenter for minimally invasive measurement and characterization of soft tissue response. *Medical Image Analysis* 2007; **11**(4): 361–373.

18. Carter FJ, Frank TG, Davies PJ, McLean D, Cuschieri A. Measurements and modelling of the compliance of human and porcine organs. *Medical Image Analysis* 2001; **5**(4): 231–236.

19. Kauer M, Vuskovic V, Dual J, Szekely G, Bajka M. Inverse finite element characterization of soft tissues, Vol. 6, 2002.

20. Rosen J, Hannaford B, MacFarlane MP, Sinanan MN. Force controlled and teleoperated endoscopic grasper for minimally invasive surgery–experimental performance evaluation, 1999.

21. Bicchi A, Canepa G, De Rossi D, Iacconi P, Scillingo EP. A sensor-based minimally invasive surgery tool for detecting tissue elastic properties, 1996.

22. Gao Z, Kim T, James DL, Desai JP. Semi-automated soft-tissue acquisition and modeling for surgical simulation, 2009.

23. Misra S, Ramesh KT, Okamura AM. Modelling of non-linear elastic tissues for surgical simulation. *Computer Methods in Biomechanics and Biomedical Engineering* 2010; **13**(6): 811–818.

24. Wilson LS, Robinson DE. Ultrasonic measurement of small displacements and deformations of tissue. *Ultrasonic Imaging* 1982; **4**(1): 71–82.

25. Birnholz JC, Farrell EE. Fetal lung development: compressibility as a measure of maturity. *Radiology* 1985; **157**(2): 495–498.

26. Gao L, Parker KJ, Lerner RM, Levinson SF. Imaging of the elastic properties of tissue-a review. *Ultrasound in Medicine & Biology* 1996; **22**(8): 959–977.

27. Manduca A, Oliphant TE, Dresner, MA, *et al*. Magnetic resonance elastography: non-invasive mapping of tissue elasticity. *Medical Image Analysis* 2001; **5**(4): 237–254.

28. Zheng Y-P, Mak AFT. An ultrasound indentation system for biomechanical properties assessment of soft tissues in-vivo, 1996.

29. Van Houten EEW, Miga MI, Weaver JB, Kennedy FE, Paulsen KD. Three-dimensional subzone-based reconstruction algorithm for MR elastography. *Magnetic Resonance in Medicine* 2001; **45**(5): 827–837.

30. Chopra R, Arani A, Huang, Y, *et al*. In vivo MR elastography of the prostate gland using a transurethral actuator. *Magnetic Resonance in Medicine* 2009; **62**(3): 665–671.

31. Miga MI. New approach to elastograph imaging: modality-independent elastography 2002: 604–611.

32. Liang Z, MacFall JR, Harrington DP. Parameter estimation and tissue segmentation from multispectral MR images, 1994.

33. Lee HP, Foskey M, Niethammer M, Krajcevski P, Lin MC. Simulation-based joint estimation of body deformation and elasticity parameters for medical image analysis. *Medical Imaging, IEEE Transactions on* 2012; **31**(11): 2156 –2168.

34. Yushkevich PA, Piven J, Hazlett, HC, *et al*. User-guided 3D active contour segmentation of anatomical structures: significantly improved efficiency and reliability. *NeuroImage* 2006; **31**(3): 1116–1128.

35. Bro-Nielsen M. Finite element modeling in surgery simulation. *Proceedings of the IEEE* 1998; **86**(3): 490–503.

36. Nocedal J, Wright SJ. *Numerical Optimization*. Springer Verlag: Springer New York, 1999.

37. Bharatha A, Hirose M, Hata, N, *et al*. et al. Evaluation of three-dimensional finite element-based deformable registration of pre- and intraoperative prostate imaging. *Medical Physics* 2001; **28**: 2551–2560.

38. Hensel JM, Ménard C, Chung, PWM, *et al*. Development of multiorgan finite element-based prostate deformation model enabling registration of endorectal coil magnetic resonance imaging for radiotherapy planning. *International Journal of Radiation Oncology, Biology and Physics* 2007; **68**(5).

39. Tanner C, Schnabel JA, Hill DLG, Hawkes DJ, Leach MO, Hose DR. Factors influencing the accuracy of biomechanical breast models. *Medical Physics* 2006; **33**: 1758–1769.

40. Si H, TetGen A. A quality tetrahedral mesh generator and three-dimensional delaunay triangulator. *Weierstrass Institute for Applied Analysis and Stochastic, Berlin, Germany* 2006.

41. Lyshchik A, Higashi T, Asato, R, *et al*. et al. Thyroid gland tumor diagnosis at US elastography1. *Radiology* 2005; **237**(1): 202–211.

42. Sobin LH, Gospodarowicz MK, Wittekind C. *TNM Classification of Malignant Tumours*. John Wiley & Sons: New York, 2011.

43. Chun TY. Coincidence of bladder and prostate cancer. *The Journal of Urology* 1997; **157**(1): 65–67.

AUTHORS' BIOGRAPHIES

Shan Yang is a PhD candidate in the GAMMA Research Lab at the University of North Carolina at Chapel Hill. She received her B.E. degree in Computer Science from Shanghai Jiao Tong University. Her research is focused on physically based simulation.

Ming Lin received her BS, MS, and PhD degrees in Electrical Engineering and Computer Science from the University of California, Berkeley. She is currently the John R. & Louise S. Parker Distinguished Professor of Computer Science at the University of North Carolina (UNC), Chapel Hill and an honorary Visiting Chair Professor (Yangtze Scholar) at Tsinghua University in Beijing, China. She has received several honors and awards, including IEEE VGTC VR Technical Achievement Award 2010 and nine best paper awards. She is a Fellow of ACM and IEEE. Her research interests include physically based modeling, real-time interactive 3D graphics, virtual environments, geometric modeling, and GPU-Computing. She has (co)-authored more than 250 refereed publications and coedited/authored four books. She is the Editor-in-Chief of IEEE Transactions on Visualization and Computer Graphics and a member of six editorial boards of scientific journals. She has served as a program/paper committee member in over 130 leading conferences and co-chaired in over 25 international conferences and workshops.